

## Supercontinuum ultra wide range confocal microscope for reflectance spectroscopy of living matter and material science surfaces

Stefano Selci,<sup>a</sup> Francesca R. Bertani, and Luisa Ferrari

*Istituto dei Sistemi Complessi, Consiglio Nazionale delle Ricerche, Via del Fosso del Cavaliere 100, Rome, 00133 Italy*

(Received 15 April 2011; accepted 27 July 2011; published online 18 August 2011)

We report the design and implementation of a new reflectance laser scanning confocal system with spectroscopy imaging capabilities. Confocal spectroscopy is achieved by using a very broad spectral range supercontinuum source capable of high precision reflectance data in the VIS-IR spectral range thanks to an almost achromatic optical layout. With this apparatus we collect each single scanning point as a whole spectrum in a continuous range, associated with the optical section imaging possibilities typical of a confocal set up. While such a microscope has been developed for bio medical analysis of human skin and other similar applications, first test results on solid samples produce spectroscopic results that, compared to analytical models based on the Abelés matrix transfer methods, show a very good agreement, opening new possibilities of a complete spectroscopic fingerprinting of samples with microscopic details. *Copyright 2011 Author(s). This article is distributed under a Creative Commons Attribution 3.0 Unported License.* [doi:10.1063/1.3631661]

### I. INTRODUCTION

Laser scanning confocal microscopy (LSCM) has become an invaluable tool for a wide range of investigations especially in the field of biological and medical sciences for imaging thin optical sections in thick samples. Fluorescence imaging and related methods (Förster Resonance Energy Transfer,<sup>1</sup> Fluorescence Lifetime Imaging Microscopy,<sup>2</sup> Fluorescence Recovery After Photobleaching,<sup>3</sup> Fluorescence Correlation Spectroscopy,<sup>4</sup> etc.) is certainly the most promising and currently more developed LSCM approach. In this framework it is possible to identify different research directions like, as not-exhaustive examples, the development of tissue imaging techniques, in vivo quantitative imaging methods, testing of functionalized fluorescent probes (Green Fluorescent Protein, trackers, auto-fluorescence), and the development of instruments and techniques towards nanoscale resolution like Stimulated Emission Depletion microscopy.<sup>5</sup> Among confocal microscopy methods, the reflectance approach has recently gained great attention especially in the field of dermatology diagnostic thanks to the possibility to image skin tissue structures at different depths using two or three different wavelengths.<sup>6</sup>

The introduction of recently commercially available supercontinuum sources, usually in combination with AOTF (acoustic optical tunable filters), has led to advances in several of these fields,<sup>7-11</sup> and opens the possibility to work in the near infrared (IR) spectral range, which has been previously used mainly to have new sources for excitation in the two-photon visible fluorescence microscopy. Recent commercial confocal laser scanning microscopes also present a spectral mode, but, since acquisition is performed via PMT or APD detection, it is possible to obtain the whole spectrum only by sequentially scanning AOTFs, prisms or gratings.

---

<sup>a</sup>Stefano.Selci@isc.cnr.it



The results here presented have been obtained by using a new supercontinuum laser scanning confocal microscope apparatus designed to perform simultaneously hyperspectroscopy in the VIS-IR range on biological and solid samples together with the usual 3D high resolution spatial imaging.

While hyperspectroscopy imaging is not a novel realization in optical microscopy, it is not a common feature in LSCM and until now has been used quite differently in other groups. For example, Shi *et al.* use the potentiality of a supercontinuum source to explore the sample with a suitable grating during acquisition, resolving single wavelengths at different depths, by the use of a well-designed chromatic sample objective.<sup>12</sup> The use of a supercontinuum source to obtain spectroscopic data has been explored quite recently also in the CLASS (Confocal Light Scattering and Absorption) projects,<sup>13–15</sup> but in this case the acquired data are analyzed as light scattering spectra based on the Mie scattering theory, in order to classify dimension and shapes of very small scatterers. Booth and al.<sup>16</sup> indeed use a supercontinuum laser source for reflectance spectroscopy by their LSCM, but the used spectral range is very small (from 500nm to 650nm) and, moreover, no effort is shown to obtain an achromatic layout. Instead, an achromatic set-up is an essential point to be sure that all the spectrally resolved features are coming from the same sample volume, otherwise spectroscopy becomes a pointless feature of the instrument.

The new LSCM here described was realized to obtain complete spectroscopic images by the acquisition of a one-shot wide range reflectance spectrum, for every image pixel in the three-dimensional sets of data typical of a confocal microscope, collecting at once the entire emission of the supercontinuum source. The achromatic set-up makes such data collection meaningful, keeping each wavelength contribution related to the same point of the sample.

In our geometry, despite the fact that the optical focus produces light scattering at all angles generated by a sub-wavelength lateral dimension, the typical LSCM tight control of the light path retains, at the end, only the pure normal-incident reflection information. In fact, experimental data have been compared to reflectance spectra generated by first-principle optics multi-layer machinery, by using the Abelès matrix transfer method,<sup>17</sup> with remarkable agreement. Moreover, the ability to precisely select the same focus position for all the available wavelengths, has permitted also back-focusing on a silicon structure below a 400 $\mu$ m thick substrate, realizing at once an instrument that it is also suitable for very specialized tasks, like failure analysis applications. The microscope has been developed with the aim to apply a typical solid state spectroscopic approach (by dielectric function classification) to the early detection of skin cancer, disease classification and similar applications. The LSCM is indeed considered to be useful in such respect,<sup>18,19</sup> also leading towards great very local and fast tools developed for this specific purpose.<sup>20</sup> We are in the middle of such an achievement, and we have yet to prove our approach useful and possible also for biologic tissues. Nevertheless, results are so promising that encourage research into other fields of application.

## II. SUPERCONTINUUM BASED CONFOCAL MICROSCOPY

The reflectance confocal microscope described here has been designed and realized completely by our research group.<sup>21</sup> As a source of illumination it uses a supercontinuum laser generated by a Nd:Yag injected in a photonic fiber and characterized by continuous emission spectrum in visible and near IR wavelength range (450 nm - 2500 nm) (NKT Photonics superKTM Power+) with a maximum power density of the order of 1.5 mW/nm.

As shown in Fig. 1, the beam is first expanded achromatically (a 4X BE04R Thorlabs expander based on protected Silver mirrors), and then directed to a 45° beam-splitter. Part of the beam is directed to an infinite conjugate reflective objective characterized by a Cassegrain-Schwarzschild design (Newport mod. 50102-02 with MgF<sub>2</sub> protected Aluminum mirrors), with a working distance of 10.4 mm and NA of 0.52, fully achromatic in a spectral range between 200 nm and 20  $\mu$ m. After sample reflection, the beam is transmitted through the beam splitter and is focused by an identical reflective objective on a home-designed piezoelectric driven variable pinhole, with an operative range between 0 and 150  $\mu$ m. The outflowing radiation is collected and converted again to a parallel beam by an off-axis parabolic 38 mm diameter mirror (Newport), then diverted to the optical bench plane and focused by another parabolic mirror. On the focal plane we have placed the entrance of an optical fiber that is connected to an array spectrometer for a spectrum recording for the VIS range

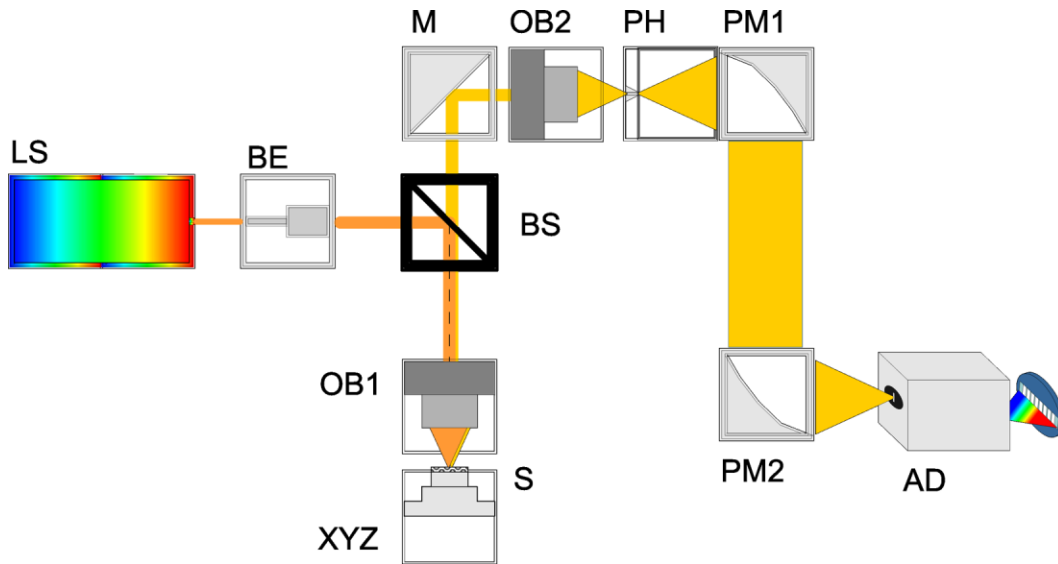


FIG. 1. LSCM schematic. LS supercontinuum laser; BE beam expander; BS beam splitter; OB1, OB2 reflective objectives; S sample; XYZ sub-micrometric stage; M plane mirror; PH pinhole; PM1, PM2 parabolic mirrors; AD array detector, with a spectrograph eventually connected by an optical fiber.

(Avantes mod. AvaSpec-2048 USB2), while for the infrared range we are using a single InGaAs detector with interference filters for wavelength selection.

The sample is scanned while keeping the beam fixed, using a combination of an XY piezoelectric table (Physik Instruments M664), that has a scanning range of 25 mm with 300 nm step resolution, and a Z stage (Newport GTS30V) with a 30 mm vertical range and  $\pm 0.1 \mu\text{m}$  repeatability, for fine focus adjustment.

We have generally used only mirror-like optical elements to avoid any chromatic aberration, except, of course, for beam-splitting where shape and materials are critical features. We have tested different optical flats, with some pros and cons for each case. For example, on thick plates some ghosting is unavoidable, and the very wide interval of wavelengths produces somewhat different paths that negatively impact the focusing on the pinhole. Note that other common beam splitters, like cubes or pellicles, can be burned out because of collection of all the available radiation coming from the laser: we can have something of the order of  $6 \text{ W/cm}^2$  deposited on the beam splitter, also after 4X beam expansion and at only 25% of the maximum laser output. Moreover, the radiation is pulsed at 5 psec with a repetition rate of 80 MHz, therefore with a further increase of a factor of 2500 of the instantaneous power deposition. Note also that we cannot reduce arbitrarily the power output. In fact, the overall spectral composition of the supercontinuum source is power dependent, being the results of complex nonlinear interactions of the Nd:Yag pump laser within the photonic optical fiber. In particular, the visible onset and the predominance of the 1064 nm line over the entire spectrum are both controlled by setting the power output. We usually work at not less than 15% of overall power. Quite obviously, a preliminary wavelength selection of a supercontinuum source, especially for fluorescence works, is a much more common choice,<sup>22</sup> and eliminates a lot of additional problems.

The results presented here have been obtained with a beam splitter made by a 6 mm thick zinc sulfide plate, also known with the commercial name of CLEARTRAN<sup>TM</sup> (by CVD inc.). This material, because of its high refractive index (2.27 at  $1 \mu\text{m}$ ), if used as beam splitter combines a high reflection, more than 15%, and low transmission, with about 13% of overall beam splitting performance. While it is transparent below  $14 \mu\text{m}$ , it can support easily UV reflection, but cannot transmit it, making it useful for fluorescence as well. However it suffers a relatively strong index of refraction variation in the visible range with an excess of chromatic ghosting, while greatly increasing the efficiency of the sample illumination because of its strong reflection. This latter feature can be

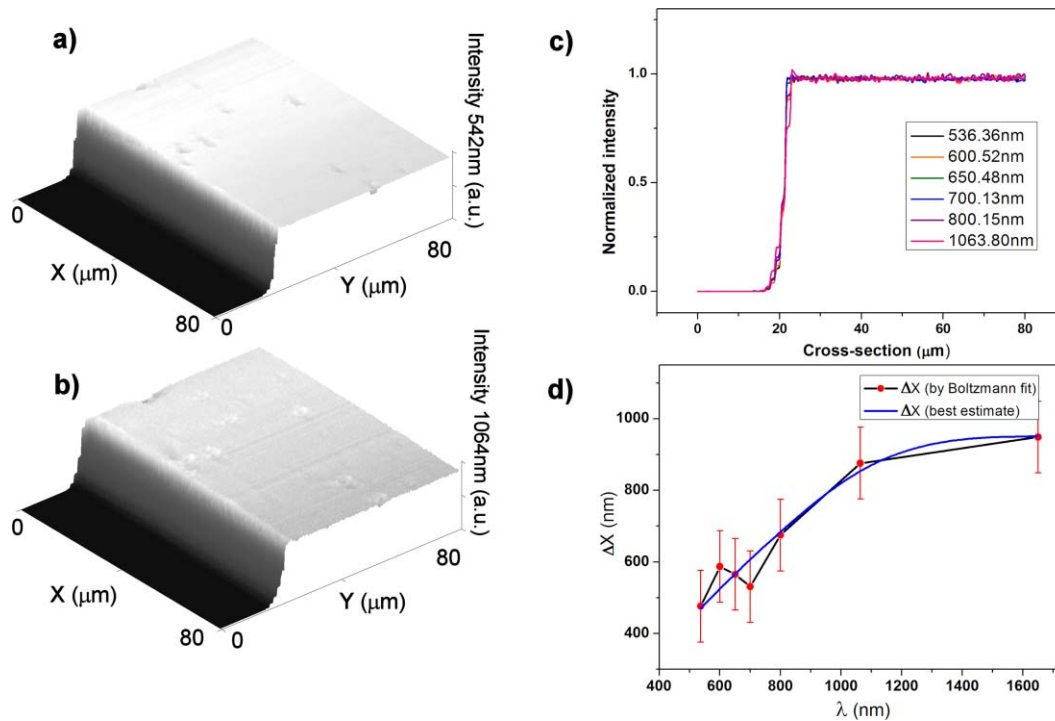


FIG. 2. The confocal image of silicon wafer edge at 542 nm in Fig. 2a) (at 1064 nm in Fig. 2b)) allows lateral resolution evaluation. A selected number of wavelengths of a single line scan is extracted, and shown in Fig. 2c). The width  $\Delta X$  of every profile has been evaluated by using a Boltzmann function shape and values shown in Fig. 2d), that includes X motion inaccuracy, together with a best fit by a quadratic curve. Note that every edge is centered in the same position, irrespective of the selected wavelength.

useful in the case of solid samples, while it can produce an excess of thermal damage for soft matter. The coupling of low NA objectives with the specifications of this material explains why our axial resolution is not state of the art, however adequate for our purposes. If we reduce noticeably the laser's first reflection on the specimen, by using a beam splitter made of more transparent materials (glass,  $\text{CaF}_2$ ), and regulate the laser well below the 25% of its maximum available power, we have run tests that prove no damage on the biological tissue (chicken skin), although the lower signal requires, in this case, better detectors.

Custom software, written in C++, allows real time control of the scanning process, data acquisition and data storage of an entire spectrum for each scanning point. For a  $512 \times 512$  points<sup>2</sup> image, and 1024 spectral points for each XY point, we need to collect 512 MB for each Z plane value (considering two bytes for each spectral element). Such huge files require specific tools to be analyzed, that are again written using C++ for efficiency and flexibility.

### III. SPECIFICATIONS AND RESULTS

The standard way to characterize LSCM apparatus is to assess lateral and vertical resolution. In the present configuration the check of the lateral resolution of our LSMC is limited by XY stage minimum step of 300 nm. As a test for lateral resolution we collect images from a cleaved edge of a silicon sample, as suggested by a previous work.<sup>23</sup> We show in Fig. 1 two images obtained from a 400 μm thick cleaved silicon wafer corresponding to the wavelengths of 542 nm (Fig. 1(a)) and 1064 nm (Fig. 1(b)), two of contemporaneously acquired 1158 images available for the same focal plane. It's easy to point out that the edge is not perfectly perpendicular to the scanning direction. Selecting one arbitrary cross-section over the edge we can compare the different resulting profiles at different wavelengths, as shown in Fig. 2(c).

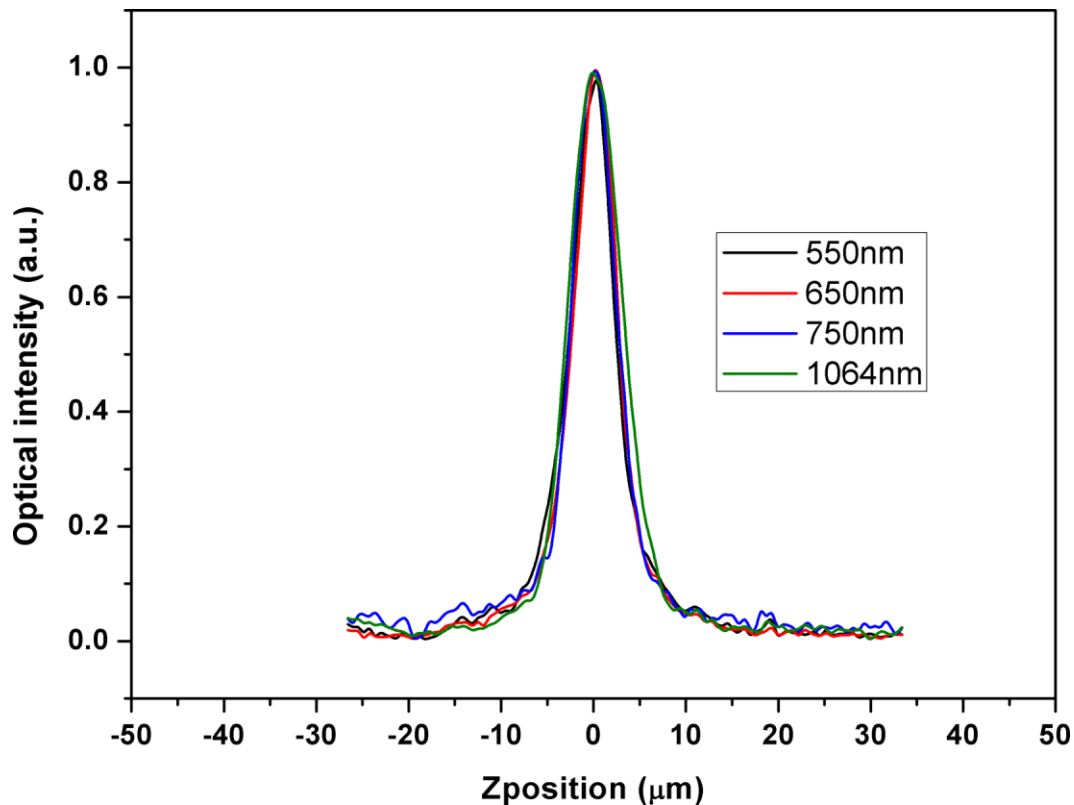


FIG. 3. Evaluating the FWHM of the optical intensity, while scanning a mirror along the Z direction at a fixed XY point, allows axial resolution definition. The shown resolution is always of the order of  $5 \mu\text{m}$ , as resulting from a Gaussian fit. The same fit produces a maximum variation of  $0.3 \mu\text{m}$  in the obtained intensity position.

Taking into account the precision and the repeatability (reported as error bars in Fig. 2(d)) of our XY scanning system, the best fit of a series of the step cross-sections by a Boltzmann function  $y = A_2 + (A_1 - A_2)/(1 + e^{(\frac{x-x_0}{dx})})$ , performed for some selected wavelengths, indicates a lateral resolution of about  $0.9 \lambda$  in the visible side of the spectrum ( $0.89 \lambda$  at  $536 \text{ nm}$ ), while we approach  $\lambda/2$  in the IR part ( $0.58 \lambda$  at  $1650 \text{ nm}$ ). The most striking feature visible in Fig. 2(c) is that no shift is visible in the silicon step cross-section as a function of wavelength within a maximum absolute error of  $0.17 \mu\text{m}$ , as coming from the same fit, proving the achromatic behavior of the microscope.

The axial resolution is estimated, as usual, by scanning a mirror at a fixed XY position over a Z range. Figure 3 shows one of the trials shown for only few wavelengths, after normalization. The FWHM of the resulting intensity curve is around  $5 \mu\text{m}$  between  $500 \text{ nm}$  and  $1.064 \mu\text{m}$ .

Again, the most relevant result is that all the wavelengths have the same focus, as demonstrated by the same peak position within  $0.3 \mu\text{m}$  after a fit with a Gaussian shape, which confirms the achromaticity of the entire optical apparatus. If the standard expressions for lateral and axial resolution<sup>24,25</sup> are used, namely  $\Delta x = 0.4\lambda/NA$  and  $\Delta z = 1.4\lambda/NA^2$ , we obtain a fair agreement using the value of  $0.52$  as NA for our reflective objective. For instance, at  $\lambda = 1.65 \mu\text{m}$  we have an estimated lateral resolution of  $0.96 \mu\text{m}$  with respect to the expected value of  $1.27 \mu\text{m}$ , while at  $\lambda = 0.536 \mu\text{m}$  we obtain  $0.48 \mu\text{m}$  with respect to the expected value of  $0.41 \mu\text{m}$ . In this latter case, however, we have to consider a systematic  $0.3 \mu\text{m}$  error in the lateral positioning due to limitations of our XY table. Generally speaking, we can expect a lateral resolution a little better than the theoretical one based on a standard Airy shaped PSF function. In fact, while the determination of the exact expected resolution of our Schwarzschild objectives is out of the scope of this paper, pupil obscuration, one of the major characteristic of Schwarzschild objectives, has been well known to be able to produce better resolved images in microscopy.

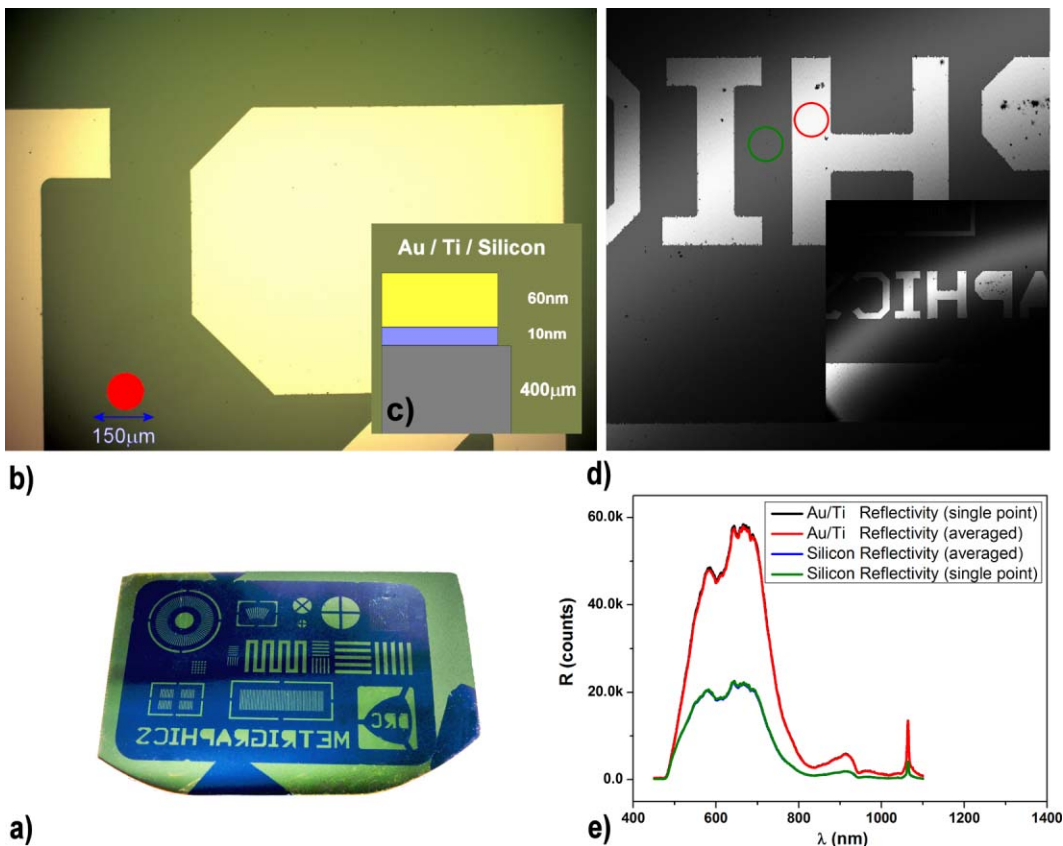


FIG. 4. A bilayer metallic deposition of Au/Ti is deposited over a  $400 \mu\text{m}$  silicon substrate and shown in picture a). A magnification made by an ordinary optical microscope is shown in b), together with a sketch of the multilayer structure (c). Two confocal images of different magnification are shown in d), respectively of  $5 \text{ mm} \times 5 \text{ mm}$ , and  $10 \text{ mm} \times 10 \text{ mm}$ . Single point or averaged reflectivity spectra, derived from the two zones marked in d), are shown in e).

## A. Results for the VIS range

As an exemplificative result that can be obtained with this microscope, we show data obtained for a test pattern realized with the mask shadowing evaporation of letters and other structures (demo by Metrigraphics LLC, USA) that has produced bi-metallic layer objects on silicon, namely by evaporation of  $10 \text{ nm}$  of titanium and  $60 \text{ nm}$  of gold over a  $400 \mu\text{m}$  silicon wafer. As we show below, our instrument gives us more than simple images, providing detailed information about the chemical composition by additional spectroscopic information. This result is obtained via the analysis of the resulting reflectivity, having assumed the complex dielectric function of different components and their thickness as given by the growth parameters.

In Fig. 4(a) it is possible to see the picture of the sample surface, in Fig. 4(b) a micro-photography, and in Fig. 4(c) a sketch of the layered structure. The confocal images obtained at  $670 \text{ nm}$  and shown in Fig. 4(d), have been acquired in two scanning ranges, namely  $5 \text{ mm} \times 5 \text{ mm}$ , sampled with  $512^2$  points, and  $10 \text{ mm} \times 10 \text{ mm}$ , sampled with  $256^2$  points. In Fig. 4(e) the available reflectivity spectra are shown for the two regions marked with colored circles. Note that no noticeable difference exists between single point reflectivity and  $600$  points area-averaged spectra. The overall shape and the intensity of every single wavelength are both the results of several factors, like the intensity distribution of the laser source, the transfer function of the microscope, and the sensitivity of the detecting spectrometer. A cumbersome normalization is always possible, for instance using a Spectralon reference or other well-known and well characterized samples. But there is another possibility.

In fact, it is possible to compute the reflectivity ratio between points of regions of different nature, that is quite easy in this case, but always possible in the more general case by adequately selecting a region of interest based on morphology or other features of the sample. With this approach, the ratio normalizes the image by itself and the so normalized reflectivity can be directly compared to analytical expressions. Because points are acquired one after each other, the laser source, the microscope and the detector are all well compensated. The first step is therefore to derive a general expression for the reflectivity of a double layer between two semi-infinite media, each medium characterized by its optical constants and thickness. Because the very wide spectral range, we have to consider a complex dielectric function for each component, obtaining an expression that is of general validity, except for the adoption of a single angle of incidence, that is, in this case, simply equal to zero. It is possible to write a formula using the Abelés matrix approach,<sup>17</sup> writing the complex reflectivity coefficient  $r$  in terms of the elements  $m_{ij}$  of a characteristic matrix:

$$r = \frac{(m_{11} + m_{12}p_N)p_1 - (m_{21} + m_{22}p_N)}{(m_{11} + m_{12}p_N)p_1 + (m_{21} + m_{22}p_N)} \quad (1)$$

Here the  $P_1(P_N)$  is the optical quantity  $p_1 = \tilde{n}_1 \cos(\theta_1)$  ( $p_N = \tilde{n}_N \cos(\theta_N)$ ) as considered for the semi-infinite medium from which the radiation is coming (the last encountered semi-infinite medium). Here we consider only normal incidence, hence no polarization is involved and transverse electric (TE) formalism is used.

Within this formalism, the optical properties of  $i$ -th specific layer are represented by the matrix  $M_i$ :

$$M_i = \begin{bmatrix} \cos(k_0 \tilde{n}_i d_i \cos(\theta_i)) & -i \sin(k_0 \tilde{n}_i d_i \cos(\theta_i)) \\ -i \sin(k_0 \tilde{n}_i d_i \cos(\theta_i)) & \cos(k_0 \tilde{n}_i d_i \cos(\theta_i)) \end{bmatrix} \quad (2)$$

where  $k_0 = 2\pi/\lambda_0$  is computed in vacuum,  $\tilde{n}_i$  is the complex dielectric function for the specific layer and  $d_i$  is its thickness. The angle  $\theta_i$  in every layer is computed by the generalized Snell law, but in this case it is merely zero. The characteristic matrix elements that enter in the expression (1) are the elements of a matrix  $M = \prod_{i=2}^{N-1} M_i$  that results from multiplication of each matrix layer, where we have assumed that the index 1 and  $N$  are reserved for the two surrounding semi-infinite media. The full expansion of (1) is quite a long exercise also for normal incidence and only two layers. For this particular case the small thickness of the two metallic layers could imply a simpler linearized version,<sup>26,27</sup> but we want to retain the full formulation as a tool for future tasks. Therefore a full analytical expansion of (1) is made with the aid of a commercial mathematical package (Maple<sup>TM</sup>), including the final conversion to a real expression of reflectivity  $R = |\tilde{r}|^2$ . The mathematical expression, several pages long, has been translated to a C function and then compiled as an independent routine. The results of such a computation are shown in Fig. 5. The optical parameters needed to perform the computation are taken by well-known reference of Palik.<sup>28</sup>

The curve labeled a) (black) in Fig. 5 is the experimental ratio between the two parts marked in Fig. 4(d). The b) (red) curve is the calculated ratio between silicon reflectivity and the full multilayer approach, including the design thicknesses, for the metallic surface. The usual normal incidence reflectivity expression is used for the silicon part:

$$\frac{(n-1)^2 + k^2}{(n+1)^2 + k^2} \quad (3)$$

The c) curve (green) is obtained using expression (3) also for the metallic part, barely considering gold as a bulk. The dotted line d) (blue) is similar to the curve b), but using a gold thickness of 70 nm instead of 60 nm, as designed and realized, simply to show how this approach is highly dependent on the parameters involved. It is clear that the best result is obtained with a full multilayer approach, although toward the infrared region no sensible difference exists between multilayer computation and bulk gold assumption. A small variation of only ten nanometers in the Au layer means a relatively great variation of the overall calculated result: reflectivity is therefore extremely sensitive to the thickness, increasing the usefulness of such a method, because this dimensional control can be

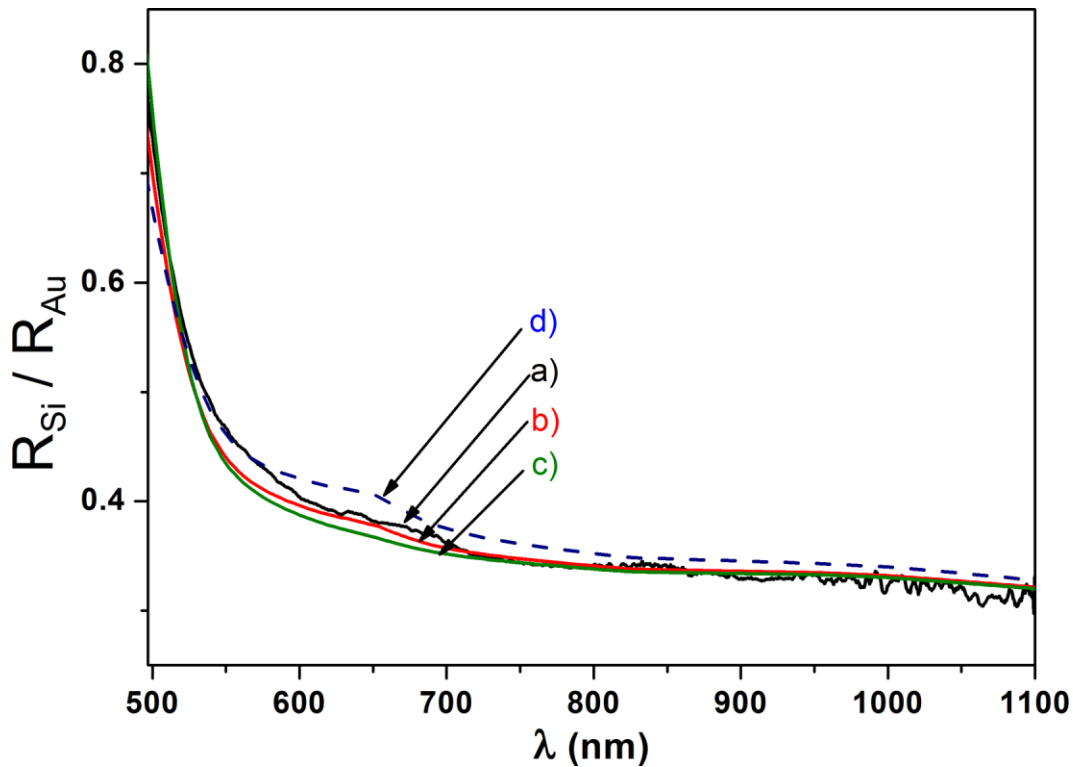


FIG. 5. The curve labeled a) (black) is the ratio between the experimental signals extracted from silicon and gold area respectively as marked in Fig. 4(d). The calculated ratios are made between the silicon reflectivity, using a semi-infinite reflectivity expression, and the reflectivity of the metallic part using a full multilayer approach (b) curve, red), or a gold semi-infinite formulation (c) curve, green), or the same as b), but intentionally changing the gold thickness from 60 nm to 70 nm (d) curve, dashed blue). Materials and parameters as in Fig. 4(c).

realized on a very local scale. A small disagreement exists in the region of 550 nm, corresponding to the region of maximum variation for the optical constants of gold. Actually, it can be considered quite a success that the shown agreement exists between experimental and calculated reflectivity ratios. Instead, there are good reasons for which optical parameters have a strong dependence on Au film preparation due to the small involved thickness, as originally known from the fundamental works of Aspnes,<sup>29</sup> and confirmed more recently.<sup>30–33</sup> The Au optical constants can have, indeed, a variation that well explain the small variation in that spectral region and could be easily computed by a best fit, if the interest is to derive the actual optical parameters of the system.

## B. Results for the IR range

As already pointed out, we can use our instrument also in the infrared region. While in the next future we will use an IR array for full spectroscopy activity, in this experiment we have used an infrared detector (Thorlabs InGaAs photodiode SM05PD4A), which, in combination with a long-pass filter, allows a detection centered at 1650 nm wavelength with a bandpass width of about 100 nm.

In this configuration, it is possible to observe the same upper patterned surface of test sample facing the objective (as shown in Fig. 5) in the IR region, but it is more interesting to turn the sample upside down, so that the patterned surface is the buried surface. In this way, focusing the light beam through the 400  $\mu\text{m}$  thick silicon substrate it is possible to look at the same structure looking from the other side of the sample (Fig. 6). This deep imaging is also possible because the used reflective objective is characterized by long working distance, which opens a world of possibilities if compared to the focus characteristics of objectives for many LSCM.

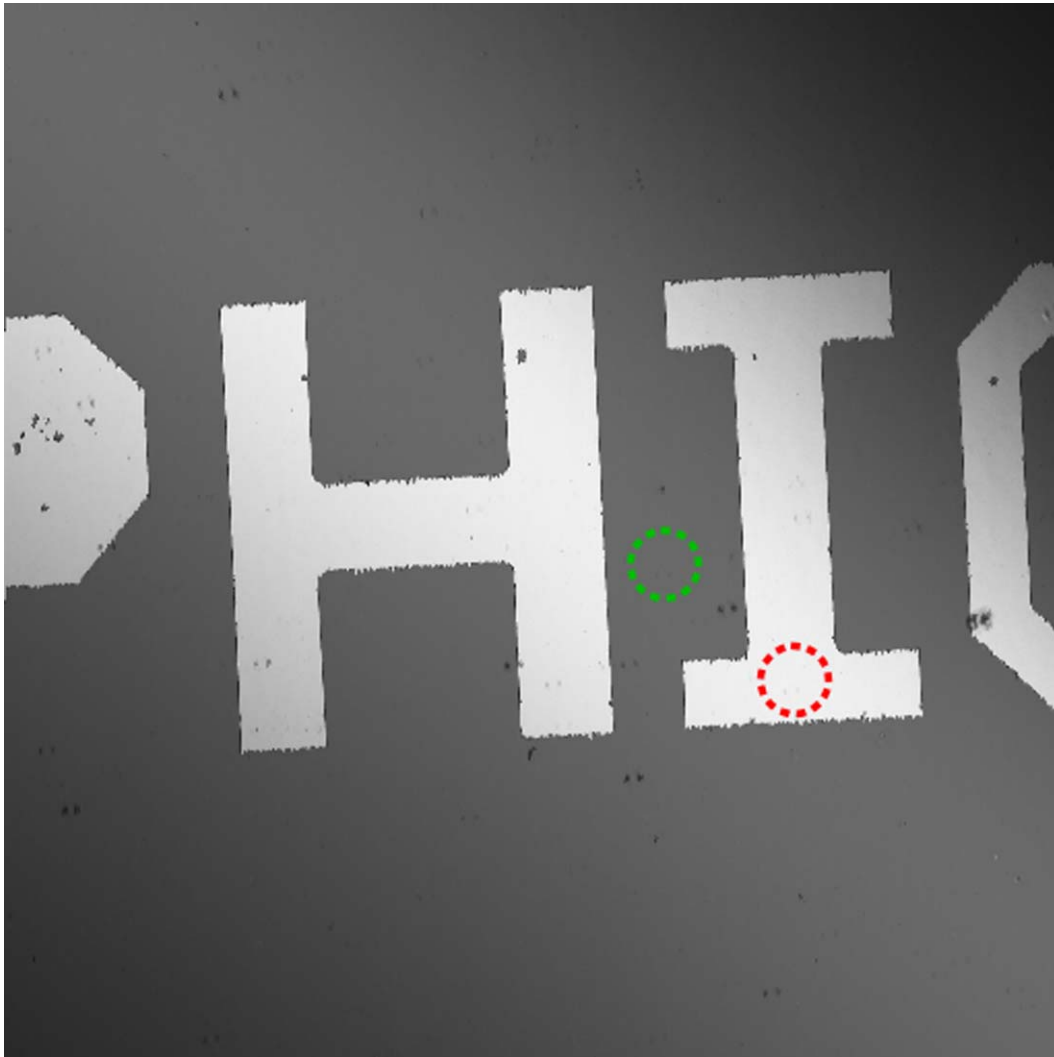


FIG. 6. Confocal image taken at 1650 nm. The same part of the sample surface seen in Fig. 4(d), that appears now mirrored, is obtained reversing the sample upside down and back-focusing through the 400  $\mu\text{m}$  of silicon thickness. The marked zones are used to compute a reflectivity ratio of 0.44, as compared to a computed value of 0.4 using the same full multilayer approach used in Fig. 5.

The experimental reflectivity ratio between zones as marked in Fig. 6 is  $R_{Si}/R_{metal}|_{\lambda=1.65\mu\text{m}} = 0.44$ , as compared to 0.4 computed with the same method as defined before. The agreement is quite good, but not as good as for data taken observing the surface upper face. Now, looking at the sample upper face the optical sequence for light propagation to the metallic part is air-gold-titanium-silicon, while just the reverse if looking to the buried patterned surface. Now, from the comparison of results shown in Fig. 5(b) and 5(c), it is clear that gold is thick enough to make the simple bulk reflection, by using expression (3), an adequate approximation, although a full multilayer approach is slightly better. On the opposite, if titanium is encountered first, the optical properties of a 10 nm film should be very close to those of a titanium bulk to realize an optimal agreement. Actually, that is not true,<sup>34</sup> as obvious for the very small thickness of the titanium film.

It is possible, however, to combine the information of the same interface as seen from two different sides of the samples and derive the best optical constants that make the best overall agreement. But all this is outside of the scope of this paper and will be the object of a subsequent work.

#### IV. CONCLUSIONS

In this paper we have presented some results of a new reflectance laser scanning confocal system that we have designed and realized. The spectroscopic imaging capabilities are achieved with the help of a very broad spectral range supercontinuum source, opening the possibility of an effective spectroscopic characterization.

On the experimental side, we can note that scanning the sample is a weak point if one considers greater scanning speeds, as requested, for instance, for biomedical applications. While we will integrate a beam scanning dispositive in the next future, the used solution is the best for large surfaces, like for semiconductor inspection or similar applications.

Also, the used detectors are good for high-reflective surfaces, but not sensitive enough for highly scattering systems, like biological ones. We have recently acquired better performing cooled CCD and InGaAs array detectors for visible and infrared ranges, to be coupled by free propagation into their respective spectrometers, therefore without an exit fiber. New results obtained with this arrangement will be available very soon.

The test results on a metallic-silicon sample have been analyzed using the classical framework of the matrix transfer method, showing a very good agreement. The fact that the agreement is quite satisfactory means that the LSCM behavior is strictly conformant to normal incidence reflectometry, with the additional advantage of superior lateral resolution and the possibility to isolate the interface of interest, thanks to the axial resolution.

If this type of analysis can be extended to highly scattering materials is an open question which we intend to answer. But, in any case, the possibility of a spectroscopic fingerprinting, via the inner normalization of the various intensities as measured within the same image, or by other methods, seems to be very accurate and really promising, also when the strict meaning of “dielectric function” cannot easily be assigned in some other specific situation.

#### ACKNOWLEDGMENTS

The activity presented has been supported by the program IDEAS-FIRB “SKINTARGET”, code RBID08W2TR, of Italian Education Minister “MIUR”. We want to thanks Dr. R. Leoni and his group of IFN-CNR for the help in the realization of the test sample.

- <sup>1</sup> Y. Sun, H. Wallrabe, S.-A. Seo, and A. Periasamy, *ChemPhysChem* **12**, 462 (2011).
- <sup>2</sup> W. Becker, A. Bergmann, M. A. Hink, K. König, K. Benndorf, and C. Biskup, *Microscopy Research and Technique* **63**, 58 (2004).
- <sup>3</sup> D. Mazza, K. Braeckmans, F. Cella, I. Testa, D. Vercauteren, J. Demeester, S. S. De Smedt, and A. Diaspro, *Biophysical journal* **95**, 3457 (2008).
- <sup>4</sup> Y. Chen, J. D. Müller, Q. Ruan, and E. Gratton, *Biophysical journal* **82**, 133 (2002).
- <sup>5</sup> S. W. Hell and J. Wichmann, *Opt. Lett.* **19**, 780 (1994).
- <sup>6</sup> K. S. Nehal, D. Gareau, and M. Rajadhyaksha, *Seminars in Cutaneous Medicine and Surgery* **27**, 37 (2008).
- <sup>7</sup> E. Auksoorius, B. R. Boruah, C. Dunsby, P. M. P. Lanigan, G. Kennedy, M. A. A. Neil, and P. M. W. French, *Opt. Lett.* **33**, 113 (2008).
- <sup>8</sup> P. M. Lanigan, C. Dunsby, J. McGinty, D. S. Elson, J. Requejo-Isidro, I. Munro, N. Galletly, B. Treanor, B. Önfelt, F. McCann, D. M. Davis, M. Neil, and P. M. French, in *An Electronically Tunable Ultrafast Laser Source Applied to Fluorescence Imaging and Fluorescence Lifetime Imaging Microscopy*, 2005 (Optical Society of America), p. CWH4.
- <sup>9</sup> D. Wildanger, E. Rittweger, L. Kastrop, and S. W. Hell, *Opt. Express* **16**, 9614 (2008).
- <sup>10</sup> C. F. Kaminski, R. S. Watt, A. D. Elder, J. H. Frank, and J. Hult, *Applied Physics B: Lasers and Optics* **92**, 367 (2008).
- <sup>11</sup> G. McConnell, *Applied Physics B: Lasers and Optics* **81**, 783 (2005).
- <sup>12</sup> K. Shi, P. Li, S. Yin, and Z. Liu, *Opt. Express* **12**, 2096 (2004).
- <sup>13</sup> H. Fang, L. Qiu, E. Vitkin, M. M. Zaman, C. Andersson, S. Salahuddin, L. M. Kimerer, P. B. Cipolloni, M. D. Modell, B. S. Turner, S. E. Keates, I. Bigio, I. Itzkan, S. D. Freedman, R. Bansil, E. B. Hanlon, and L. T. Perelman, *Appl. Opt.* **46**, 1760 (2007).
- <sup>14</sup> P. Huang, M. Hunter, and I. Georgakoudi, *Appl. Opt.* **48**, 2595 (2009).
- <sup>15</sup> I. Itzkan, L. Qiu, H. Fang, M. M. Zaman, E. Vitkin, I. C. Ghiran, S. Salahuddin, M. Modell, C. Andersson, L. M. Kimerer, P. B. Cipolloni, K.-H. Lim, S. D. Freedman, I. Bigio, B. P. Sachs, E. B. Hanlon, and L. T. Perelman, *Proceedings of the National Academy of Sciences* **104**, 17255 (2007).
- <sup>16</sup> M. Booth, R. Juškaitis, and T. Wilson, *Journal of the European Optical Society - Rapid publications* **3**, 08026 (2008).
- <sup>17</sup> M. Born and E. Wolf, *Principles of Optics: Electromagnetic Theory of Propagation, Interference and Diffraction of Light (7th Edition)* (Cambridge University Press, 1999).

- <sup>18</sup> K. Carlson, M. Chidley, K.-B. Sung, M. Descour, A. Gillenwater, M. Follen, and R. Richards-Kortum, *Appl. Opt.* **44**, 1792 (2005).
- <sup>19</sup> B. Masters and P. So, *Opt. Express* **8**, 2 (2001).
- <sup>20</sup> C. L. Arrasmith, D. L. Dickensheets, and A. Mahadevan-Jansen, *Opt. Express* **18**, 3805 (2010).
- <sup>21</sup> *Vol. RM2010A000286*, G01N ed., edited by CNR (ITALY, 2010).
- <sup>22</sup> R. Mercatelli, S. Soria, G. Molesini, F. Bianco, G. Righini, and F. Quercioli, *Opt. Express* **18**, 20505 (2010).
- <sup>23</sup> M. Gu, C. J. R. Sheppard, and X. Gan, *J. Opt. Soc. Am. A* **8**, 1755 (1991).
- <sup>24</sup> T. R. Corle, C. H. Chou, and G. S. Kino, *Opt. Lett.* **11**, 770 (1986).
- <sup>25</sup> C. J. R. Sheppard and T. Wilson, *Opt. Lett.* **3**, 115 (1978).
- <sup>26</sup> S. Selci, F. Ciccacci, G. Chiarotti, P. Chiaradia, and A. Cricenti, *Journal of Vacuum Science & Technology A: Vacuum, Surfaces, and Films* **5**, 327 (1987).
- <sup>27</sup> S. Selci, A. Cricenti, A. C. Felici, C. Goletti, and G. Chiarotti, *Physical Review B* **44**, 8327 (1991).
- <sup>28</sup> E. Palik, *Handbook of Optical Constants of Solids (5 Volume Set)* (Academic Press}, 1997).
- <sup>29</sup> D. E. Aspnes, E. Kinsbron, and D. D. Bacon, *Physical Review B* **21**, 3290 (1980).
- <sup>30</sup> S. A. Kovalenko and M. P. Lisitsa, *Semiconductor Physics, Quantum Electronics & Optoelectronics* **4**, 352 (2001).
- <sup>31</sup> S. A. Kovalenko and M. P. Lisitsa, *Semiconductor Physics, Quantum Electronics & Optoelectronics* **5**, 294 (2002).
- <sup>32</sup> W.-J. Lee, J.-E. Kim, H. Y. Park, S. Park, M.-s. Kim, J. T. Kim, and J. J. Ju, *Journal of Applied Physics* **103**, 073713 (2008).
- <sup>33</sup> V. B. Svetovoy, P. J. van Zwol, G. Palasantzas, and J. T. M. De Hosson, *Physical Review B* **77**, 035439 (2008).
- <sup>34</sup> A. D. Rakic, A. B. Djurišić, J. M. Elazar, and M. L. Majewski, *Appl. Opt.* **37**, 5271 (1998).